Conformal field theory of the Flory model of polymer melting

Jesper Lykke Jacobsen*
Laboratoire de Physique Théorique et Modèles Statistiques, Université Paris–Sud, Bâtiment 100, F-91405 Orsay, France

Jané Kondev†
Physics Department, MS057, Brandeis University, Waltham, Massachusetts 02454, USA
(Received 26 January 2004; published 4 June 2004)

We study the scaling limit of a fully packed loop model in two dimensions, where the loops are endowed with a bending rigidity. The scaling limit is described by a *three-parameter* family of conformal field theories, which we characterize via its Coulomb-gas representation. One choice for two of the three parameters reproduces the critical line of the exactly solvable six-vertex model, while another corresponds to the Flory model of polymer melting. Exact central charge and critical exponents are calculated for polymer melting in two dimensions. Contrary to predictions from mean-field theory we show that polymer melting, as described by the Flory model, is *continuous*. We test our field theoretical results against numerical transfer matrix calculations.

DOI: 10.1103/PhysRevE.69.066108 PACS number(s): 05.50.+q, 05.20.−y

I. INTRODUCTION

Over the years, polymers physics has greatly benefited from studies of lattice models. One persistent theme has been the use of lattice models to uncover universal properties of chain molecules. An example is provided by the scaling exponents which characterize the statistical properties of polymer conformations, in the limit of very long chains [1]. For polymer chains confined to live in two dimensions, exact values of exponents were calculated by Nienhuis [2] using the self-avoiding walk on the honeycomb lattice. The predicted value of the swelling exponent, which relates the linear size of the polymer to the number of monomers, was directly measured in recent fluorescence microscopy studies of DNA absorbed on a lipid bilayer [3].

Here we turn to the problem of polymer melting, which deals with a possible phase transition induced by the competition between chain entropy and bending rigidity. Bending rigidity determines the persistence length of the polymer. This is the distance over which the relative orientations of two chain segments are decorrelated due to thermal fluctuations. The long chain limit mentioned in the previous paragraph is obtained when the polymer length is much greater than its persistence length.

It is important to point out that the effect of finite bending rigidity depends crucially on the steric constraints imposed on the polymer by its interactions with the solvent. For example, in the presence of a good solvent the polymer is in a "dilute" phase. Typical chain conformations are swollen with empty space between the monomers filled by solvent molecules. On the lattice, the dilute phase is characterized by a vanishing fraction of sites occupied by monomers. In this phase, the bending rigidity simply increases the persistence length of the polymer, and it does not lead to a phase transition. This can be verified analytically in two dimensions, within the framework of Nienhuis' self-avoiding walk model [4,5].

The picture changes considerably when the polymer is in a "compact" phase, with the monomers occupying all the available space. Such a situation is relevant, for instance, when modeling the conformations of globular proteins [6]. Compactness in this case follows from the interaction between hydrophobic amino acids and the solvent (water), which leads to the expulsion of the solvent from the bulk of the protein. The simplest way to model this effect is to enforce compactness as a global, steric constraint on the polymer configurations [6]. Within this compact phase, one expects a phase transition from a disordered melt to an ordered crystal as the stiffness of the polymer is increased.

To study this melting transition, in 1956 Flory introduced a lattice model [7]. Flory's model, in its simplest formulation, consists of a single chain, described by a self-avoiding walk on the square lattice, endowed with a bending rigidity. To describe the melted phase the chain is taken to be maximally compact, filling all the sites of the square lattice; see Fig. 1. The resistance to bending is modeled by an energy penalty for making 90° turns.

In the Flory model, at infinite temperature the entropy dominates and the polymer will exhibit a finite density of bends, as in Fig. 1(a). As the temperature is lowered to zero, all the bends are expelled from the bulk and their density goes to zero, as in Fig. 1(b). The nature of the transition from the high temperature melt to the low temperature crystal has been debated over the years [8]. Here we show that the melting transition is *continuous* and calculate exact values of scaling exponents at the transition.

In his original paper, Flory [7] proposed a mean-field treatment which predicts a first-order transition. According to Ref. [7], the density of bends goes to zero at the transition and the chain entropy vanishes. This prediction of a first-order transition with a vanishing entropy was challenged by Nagle [9]. Namely, he showed that the exactly solvable six-vertex model maps to a related polymer model which differs from Flory's by the presence of polymer loops of all sizes. Applying Flory's mean-field approximation to this model

*Email address: jacobsen@ipno.in2p3.fr
†Email address: kondev@brandeis.edu

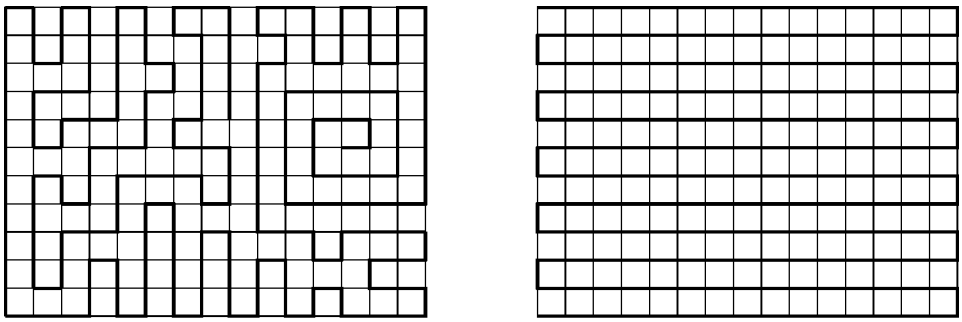

FIG. 1. Compact polymer configurations on an 11×15 square lattice: (a) Typical configuration in the melt phase, and (b) zero-temperature crystalline state, in which the number of bends is minimum.

leads once again to the prediction of a first-order melting transition. However, as Nagle pointed out, this is at odds with the exact solution of the six-vertex model [10] which predicts a continuous, infinite order transition. This observation makes it questionable that the Flory approach is valid in the original model as well. In fact, a few years later Gujrati and Goldstein [11] proved that the polymer entropy in Flory's model stays finite all the way down to zero temperature when it finally vanishes. However, the order of the transition still remained an unresolved question.

Monte Carlo simulations of Baumgartner and Yoon [12], where they allowed for many chains and a finite density of empty sites, showed a first-order melting transition. Soon thereafter Saleur [13], using a transfer matrix approach, presented numerical evidence of a continuous transition, similar to the one found in the six-vertex model. The analogy with the six-vertex model points at the possibility of having a high-temperature phase with continuously varying exponents. A few years later, Bascle, Garel, and Orland [14] proposed an improved mean-field treatment of the Flory model, which does not suffer from the problem of a vanishing entropy at the transition. It also predicts a first-order transition. This is however at odds with more recent Monte Carlo work by Mansfield [15] which, although strictly speaking dealing with a system of many chains, is again in favor of a continuous transition.

Here we show that polymer melting is continuous, as originally argued by Saleur [13], by making use of a particular model, the *semiflexible loop* (SFL) *model*, and its height representation. Furthermore, we calculate the central charge and exact scaling exponents at the transition. These results are checked against detailed numerical transfer matrix computations.

The SFL loop model can be thought of as a "loop generalization" of the so-called F model [9], in which suitably defined loops carry additional Boltzmann weights. The F model is a special case of the six-vertex model [10], in which all vertices carry equal weights. This connection will serve as the motivation for introducing a more general model, the *generalized six-vertex model*, in which the general (zero-field) six-vertex model is endowed with extra loop weights. We shall finally introduce a similarly generalized version of the eight-vertex model [10]. Its interest from a polymer point of view is that it allows for a unified description of semiflexible lattice polymers in a variety of phases: compact, dense, and dilute. Furthermore, it allows us to discuss the effect of vacancies on the polymer melting transition.

The paper is organized as follows. In the following section we introduce the SFL model, which, in the limit of zero loop weight, gives the Flory model of polymer melting, and we discuss its phase diagram. In Sec. III we discuss the height representation of the loop model and how it leads to a conformal field theory in the scaling limit. We make use of the field theory in Sec. IV to calculate the central charge and scaling exponents, which we check against numerical transfer matrix computations in Sec. V. In Sec. VI we propose a phase diagram for the generalized six-vertex and eight-vertex models. We end with a discussion of the scaling of semiflexible compact polymers, and we argue that the generalized eight-vertex model furnishes a rather complete description of noncompact semiflexible polymers. An appendix is reserved for a detailed discussion of the construction of the transfer matrices.

II. SEMIFLEXIBLE LOOP MODEL

Here we define the SFL model, and give a rough sketch of its phase diagram based on the limits of weak and strong bending rigidity. The fact that the SFL model reduces to the F model in the limit of unit loop fugacity [9] plays an important role in guiding our intuition about the loop model. It also provides an exactly solvable line in the phase diagram, against which the field theoretical and numerical results can be checked.

A. Definition of the model

The semiflexible fully packed loop model on the square lattice (the SFL model) is defined by filling the square lattice with loops drawn along the lattice edges. Allowed loop configurations satisfy two constraints: (a) self avoidance—loops are not allowed to cross, and (b) full packing—every site is visited by exactly one loop.

On the square lattice with periodic boundary conditions, edges that are not covered by loops also form loops, as there are two unoccupied edges associated with every site of the lattice. We refer these to as "ghost loops."

Given the configurations of the semiflexible loop model, the Boltzmann weights are defined in the following way. Every real loop is given a weight n_{b}, and every ghost loop has weight n_{g}. (In all the figures the real and ghost loops are shown as black and gray, respectively, whence the subscripts b and g.) The parameters n_{b} and n_{g} act as fugacities of the two-loop flavors, and as such they control the average num-

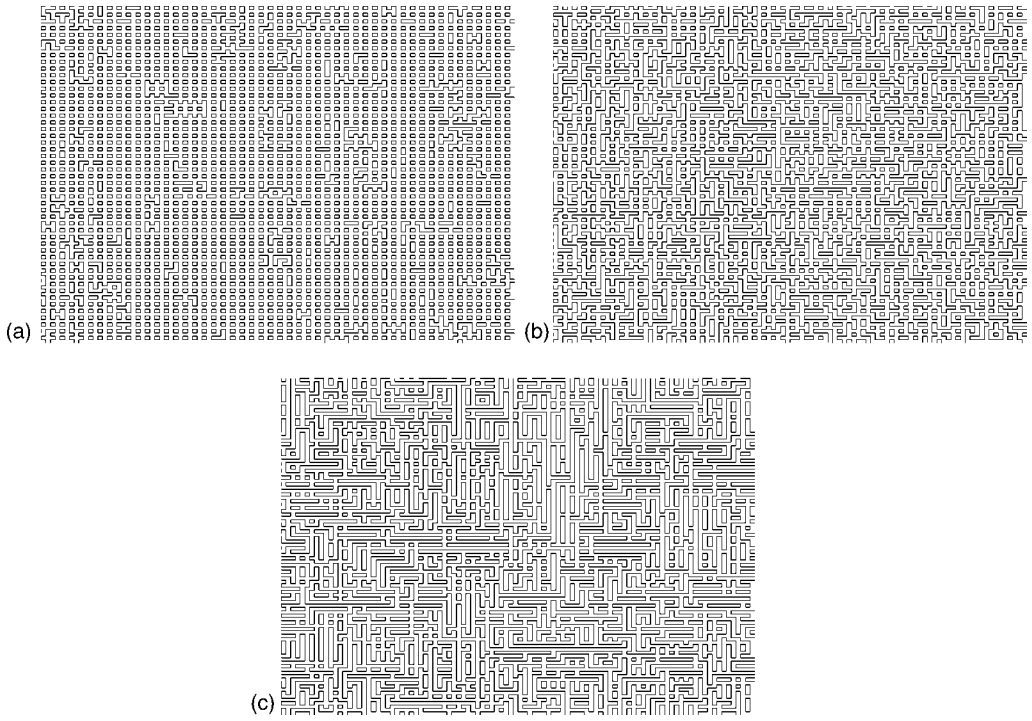

FIG. 2. Typical configurations in the SFL model with $n_b = n_g = 2$ and bending rigidity parameter $w_X = 1/4$ (a), $w_X = 1$ (b), and $w_X = 4$ (c). We shall show that the left and middle panels correspond to critical melt states, while the right panel is a noncritical crystalline state. In the latter, domains of nonzero staggered polarization (see Sec. II B 2) are clearly visible.

ber of loops of each flavor [16]. They can be varied independently as the number of ghost loops is not fixed by the number of real loops [17]. Furthermore, a weight w_X is assigned to each vertex of the lattice at which the real and ghost loops cross. For $w_X > 1$ this has the effect of disfavoring vertices at which the loop makes a 90° bend, or, in other words, the loops are semiflexible. The partition function of the semiflexible loop model is

$$Z = \sum_{\mathcal{G}} n_b^{N_b} n_g^{N_g} w_X^V, \tag{1}$$

where the sum runs over all allowed loop configurations $\mathcal{G}$. N_b and N_g are the number of real and ghost loops, respectively, while V is the number of crossing vertices; these are the two rightmost vertices in Fig. 3. In the limit $n_b \to 0$, with $n_g = 1$, we recover the Flory model: Z/n_b counts compact polymer loops each weighed by w_X^V.

The semiflexible loop model can be thought of as the generalization of the fully packed loop model on the square lattice (FPL^2) model introduced in Ref. [17]. The FPL^2 model is given by the partition function, Eq. (1), with $w_X = 1$. It has a critical phase for $|n_b|, |n_g| \leqslant 2$, characterized by a power-law distribution of loop sizes. For other values of the loop weights the model is noncritical with a distribution of loop sizes cut off at a finite value (fixed by the correlation length). Below we will show that the vertex weight w_X, for each point in the critical phase of the FPL^2 model, produces a line of fixed points which terminates in a Kosterlitz-Thouless transition.

B. Qualitative phase diagram

Rough, qualitative features of the phase diagram of the semiflexible loop model can be deduced from the limits of zero and infinite bending rigidity. The motivation for developing a precise theory of the phase diagram, as mentioned in the Introduction, stems from the interest in the $n_b \to 0$, $n_g = 1$ case, which is the Flory model of polymer melting. We are also motivated by the relation of the SFL model to the integrable six-vertex model, and its generalizations.

1. Flory model

In the Flory limit of the SFL model, the $w_X = 1$ point is the compact polymer problem, which we have studied previously [17]. Here one is concerned with enumerating all self-avoiding walks that visit every site of the lattice. We have shown that compact polymers on the square lattice are a critical geometry characterized by non-mean-field scaling exponents which can be calculated exactly from a field theory.

As w_X is increased away from one, we are dealing with a compact polymer with a bending rigidity. In the limit $w_X \to \infty$ we arrive at a frozen phase in which the density of vertices at which the polymer bends goes to zero. This is the polymer crystal. At an intermediate weight $w_X = w_X^c (1 < w_X^c < \infty)$ there will be a melting transition. One of the important unresolved problems is the nature of this transition. Here we construct an effective field theory of the Flory model and show that the melting transition is *continuous*.

Another interesting issue is the region of $0 \leqslant w_X < 1$. As $w_X \to 0$, straight-going vertices are completely suppressed,

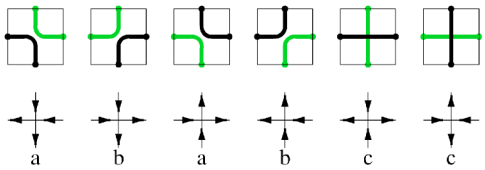

FIG. 3. Correspondence between the vertices of the six-vertex model and the FPL^2 model (here shown for an even vertex; at odd vertices the arrows are reversed).

and with appropriate boundary conditions the only allowed configurations are those of a checkerboard pattern of small loops, each loop having its minimal length of 4. If the Flory limit ($n_b \to 0$) is taken before the $w_X \to 0$ limit, there has to be a number of straight-going vertices at the boundary, the dominant configurations being those of a single wiggly line. In any case, the $w_X \to 0$ limit is again a crystalline phase of zero entropy. We shall however argue below that the corresponding crystallization transition is located at $w_X = 0$ and is thus rather uninteresting.

A qualitative idea of the physics underlying the phase diagram of the SFL model can be obtained by looking at some typical configurations for various values of w_X; see Fig. 2. The images were obtained by performing Monte Carlo simulations on a square lattice of size 100×100 with toroidal boundary conditions. For technical reasons [18] we take $n_b = n_g = 2$ and no loops of noncontractible topology are allowed. (Further details on the algorithm used for these simulations can be found in Ref. [18].)

2. Six-vertex model

Before turning our sights to the semiflexible loop model it is instructive to review exact results for the (zero-field) six-vertex (6V) model. The 6V model corresponds to the $n_b = n_g = 1$ line in the phase diagram of the SFL model. The mapping between the two is simple: at even (odd) vertices the edges covered by the real loops are identified with arrows pointing out (in), while the edges covered by the ghost loops correspond to arrows pointing in (out); see Fig. 3. The appropriate six-vertex weights are $a = b = 1$ and $c = w_X$ [19].

In the 6V model there is an order-disorder transition as a function of the vertex weight w_X. In the ordered state, which is obtained for $w_X \to \infty$, all the vertices are of the c variety (cf. Fig. 3). The order parameter is the staggered polarization, which in the loop language can be expressed as the difference between the number of horizontal and the number of vertical loop-covered edges per site [13]. The exact solution of the six-vertex model predicts a continuous (infinite-order) transition occurring at $w_X = 2$ [10]. The disordered phase for $0 < w_X < 2$ is critical with an infinite correlation length and power-law correlations. Below we will show that there is an analogous transition in the semiflexible loop model, as w_X is varied, for all values of $|n_b|, |n_g| \leqslant 2$, including the Flory case ($n_b \to 0, n_g = 1$). In the Flory model this was observed previously by Saleur in numerical transfer matrix computations [13]. For the critical phase of the model we shall construct an effective field theory using the interface representation of the loop model. This leads to exact (but nonrigorous) results for the central charge and scaling dimensions, which we confirm via numerical transfer matrix calculations.

III. FIELD THEORY CONSTRUCTION

To construct a field theory for the critical phase of the SFL model we make use of the height representation of the FPL^2 model. This was already described in detail in our previous work [17], and here it is briefly reviewed for completeness. The main effect of the vertex weight w_X on the field theory is to renormalize one of its coupling (elastic) constants. This does not change the central charge, but leads to continuously varying scaling dimensions for a specific subset of operators, which we identify. These results are confirmed by our numerical transfer matrix computations.

A. Height map

The height mapping is defined on the space of oriented loop configurations $\{\mathcal{G}'\}$. We associate $2^{N_g+N_b}$ oriented loop configuration $\mathcal{G}'$ with each loop configuration $\mathcal{G}$ of the SFL model by independently orienting every real and every ghost loop clockwise or counterclockwise.

The Boltzmann weight of an oriented loop is $\exp(i\phi)$, where the phase $\phi = \pm \pi e_b$ for clockwise (counterclockwise) oriented real loops, and $\phi = \pm \pi e_g$ for the two orientations of the ghost loops. To recover n_b and n_g for the loop weights, after summing over the two possible orientations we must set

$$n_b = 2\cos(\pi e_b), \qquad n_g = 2\cos(\pi e_g). \tag{2}$$

This particular partition of the loop weights between the two orientations has the advantage of allowing the loop weights to be distributed among all the vertices that the loop visits, thus rendering the weights local. This is achieved by assigning the phase $\pi e_b/4$ ($\pi e_g/4$) to every vertex at which the oriented real (ghost) loop makes a right turn, and the opposite phase for left turns. The fact that for every closed loop on the square lattice the difference between the number of left and right turns is ± 4, is what makes these vertex weights work. The total vertex weight is then given by the product of phase factors when the loops bend, while a weight w_X is assigned to vertices at which the loops do not bend.

Turning back to the height map, we define microscopic heights $\mathbf{h}(\mathbf{x})$ on the lattice $\{\mathbf{x}\}$ dual to the square lattice on which the loops are defined. Once the height at the origin is fixed, the heights on all the other vertices of the dual lattice are uniquely specified by the oriented loop configuration. Namely, the height difference between nearest-neighbor vertices of the dual lattice is **A**, **B**, **C**, or **D**, depending on the state of the edge that separates them. The four height-difference vectors, also referred to as "colors," are associated with the four possible states of any given edge, which can be either covered by a real or a ghost loop, with one of two possible loop orientations. Real loops are formed by alternating cycles of **A** and **B** colored edges, while the **C** and **D** colored edges are ones visited by the ghost loops. Note that

the difference between an **ABAB**$\cdots$ and a **BABA**$\cdots$ cycle encodes the orientation of the corresponding (real) loop.

The fully packing constraint and the requirement that the height be unique (i.e., the sum of height differences along any closed lattice path must be zero) imposes a single algebraic constraint on the four colors: $\mathbf{A}+\mathbf{B}+\mathbf{C}+\mathbf{D}=0$. It follows that only three of the four vectors are linearly independent. A convenient choice that respects the symmetries between the four colors is to let the corresponding vectors point from the center to the vertices of a regular tetrahedron:

$$\mathbf{A}=(-1,+1,+1), \quad \mathbf{B}=(+1,+1,-1),$$
$$\mathbf{C}=(-1,-1,-1), \quad \mathbf{D}=(+1,-1,+1). \tag{3}$$

The effective field theory for the SFL model describes the fluctuations of the coarse-grained heights which retains only the long-wavelength (much larger than the lattice spacing) Fourier modes of the microscopic heights.

B. Effective field theory: $w_X=1$

For $w_X=1$ we have the familiar case of the fully packed loop model on the square lattice. Its effective field theory was discusses in a previous publication [17] and here it is reviewed for completeness.

The partition function of the loop model in the height representation can be written as a path integral over the coarse grained heights with the (dimensionless) action:

$$S=S_E+S_B+S_L. \tag{4}$$

This action only takes into account the long-wavelength fluctuations of the microscopic height. The three terms in the action are of different origin.

The elastic term

$$S_E=\frac{1}{2}\int d^2\mathbf{x}\{K_{11}[(\boldsymbol{\partial} h^1)^2+(\boldsymbol{\partial} h^3)^2]+2K_{13}(\boldsymbol{\partial} h^1\cdot\boldsymbol{\partial} h^3) + K_{22}(\boldsymbol{\partial} h^2)^2\} \tag{5}$$

accounts for the height fluctuations due to the entropy of fully packing the square lattice with oriented loops. Equivalently, this is the entropy of edge coloring the square lattice with four different colors. The elastic term favors oriented loop configurations that minimize the variance of the microscopic height; these are the macroscopically flat states. In terms of the color degrees of freedom the flat states have the property that the four edges of each elementary plaquette are colored by two colors only.

The particular form of the matrix of elastic constants $\mathbf{K}$ is fixed by the lattice symmetries and symmetries associated with permuting the colors **A**, **B**, **C**, and **D**. The elastic constants K_{ij} are functions of the loop fugacity. For the $w_X=1$ case they were calculated in Ref. [17] using the loop ansatz [22], which allows one to identify the marginal screening charges [23]. For the FPL^2 model there are four screening charges:

$$\mathbf{e}^{(1)}=(-\pi,0,+\pi),$$
$$\mathbf{e}^{(2)}=(-\pi,0,-\pi),$$
$$\mathbf{e}^{(3)}=(-\pi,+\pi,0),$$
$$\mathbf{e}^{(4)}=(-\pi,-\pi,0). \tag{6}$$

These electric charges are associated with the most relevant vertex operators appearing in the Fourier expansion of the operator conjugate to the loop weight [see Eq. (12) below].

Demanding that all four charges have scaling dimension equal to 2 gives [using Eq. (16)]

$$K_{11}=\frac{\pi}{8}(2-e_g-e_b),$$
$$K_{13}=\frac{\pi}{8}(e_b-e_g), \tag{7}$$
$$K_{22}=\frac{\pi}{2}\frac{(1-e_b)(1-e_g)}{2-e_b-e_g}$$

for the elastic constants of the FPL^2 model; e_b and e_g satisfy Eq. (2) and take their values on the interval $[0,1/2]$. Below we will argue that the effect of $w_X\neq 1$ is to change the value of the elastic constant K_{22} while leaving the other two unchanged.

The boundary term in the action,

$$S_B=\frac{i}{4\pi}\int d^2\mathbf{x}[\mathbf{e}_0\cdot\mathbf{h}(\mathbf{x})]\rho(\mathbf{x}), \tag{8}$$

enforces the correct weight of topologically nontrivial loops. If the oriented loop model is defined with periodic boundary conditions along one direction (i.e., on a cylinder) these would be the loops that completely wind around the cylinder [24]. On a cylinder the scalar curvature ρ is nonzero only at the two boundaries at infinity. S_B has the effect of placing background electric charges $\pm\mathbf{e}_0$ at the two boundaries, where the identification

$$\mathbf{e}_0=-\frac{\pi}{2}(e_g+e_b,0,e_g-e_b) \tag{9}$$

comes about by demanding that the oriented winding loops be assigned correct phase factors, $\exp(\pm i\pi e_b)$ or $\exp(\pm i\pi e_g)$ [17].

The third term, called the Liouville term,

$$S_L=\int d^2\mathbf{x}w[\mathbf{h}(\mathbf{x})], \tag{10}$$

owes its existence to the complex weights associated with oriented loops in the bulk. The local redistribution of the loop weights made in Sec. III A leads to complex vertex weights, which in turn depend only on the colors of the four edges around the vertex. If we write the vertex weight as $\exp(-w)$, then

$$w(\mathbf{B},\mathbf{C},\mathbf{A},\mathbf{D}) = 0,$$

$$w(\mathbf{B},\mathbf{D},\mathbf{A},\mathbf{C}) = 0,$$

$$w(\mathbf{A},\mathbf{B},\mathbf{C},\mathbf{D}) = \mp i\frac{\pi}{4}(e_g + e_b),$$

$$w(\mathbf{B},\mathbf{A},\mathbf{C},\mathbf{D}) = \mp i\frac{\pi}{4}(e_g - e_b), \tag{11}$$

$$w(\mathbf{A},\mathbf{B},\mathbf{D},\mathbf{C}) = \mp i\frac{\pi}{4}(e_b - e_g),$$

$$w(\mathbf{B},\mathbf{A},\mathbf{D},\mathbf{C}) = \mp i\frac{\pi}{4}(-e_b - e_g);$$

the top (bottom) sign is for even (odd) vertices, and the colors are listed in order, starting from the leftmost edge and proceeding clockwise around the vertex. The weight operator w is invariant under cyclic permutations of the colors and it is a periodic function of the heights around a vertex. In the scaling limit the vertex weights give rise to the operator $w[\mathbf{h}(\mathbf{x})]$ in Eq. (10) which can be written as a Fourier series

$$w[\mathbf{h}(\mathbf{x})] = \sum_{\mathbf{e}\in\mathcal{R}_w^*} \tilde{w}_{\mathbf{e}} \exp\left[i\mathbf{e}\cdot\mathbf{h}(\mathbf{x})\right]. \tag{12}$$

The electric charges $\mathbf{e}$ appearing in the Fourier expansion are dictated by the lattice of periodicities $\mathcal{R}_w$ of the operator $w[\mathbf{h}]$; $\mathcal{R}_w^*$ is the reciprocal lattice. $\mathcal{R}_w$ is determined by inspection of the values the loop weight operator takes on the flat states: vectors in $\mathcal{R}_w$ connect flat states on which the loop weight operator takes identical values. The most relevant charges in $\mathcal{R}_w^*$ are the four given in Eq. (6). We identify them with the screening charges [23] of the Coulomb gas. This is the content of the loop ansatz introduced in Ref. [22].

C. Effective field theory: $w_X \neq 1$

For the SFL model, when $w_X \neq 1$, the Liouville term in Eq. (4) is modified, while the elastic and the boundary terms are unchanged. The number of marginal screening charges appearing in Eq. (12) is reduced from four to two, and the loop ansatz fixes the values of K_{11} and K_{13} only. They do not depend on the value of w_X and are given by the $w_X = 1$ formulas, Eq. (7). K_{22}, on the other hand, is a nonuniversal function of w_X. Below we present arguments for this scenario, which is supported by exact results available in the 6V case (i.e., for $n_b = n_g = 1$), and by our numerical transfer matrix calculations described in Sec. V below.

The new vertex weight w_X changes the value of w in Eq. (11) from 0 to $-\ln w_X$ for the vertex states $(\mathbf{B},\mathbf{C},\mathbf{A},\mathbf{D})$, $(\mathbf{B},\mathbf{D},\mathbf{A},\mathbf{C})$, and six other related to these two by cyclic permutations of the colors. The weights of the other 16 vertex states are unchanged. We consider the consequences of this change on the effective field theory.

In the height representation of the SFL model, the change in vertex weight corresponds to adding

$$S_X = \int d^2\mathbf{x}\, X[\mathbf{h}(\mathbf{x})] \tag{13}$$

to the action. The X operator takes the value $\ln w_X$ on the flat states made up of $(\mathbf{B},\mathbf{C},\mathbf{A},\mathbf{D})$ or $(\mathbf{B},\mathbf{D},\mathbf{A},\mathbf{C})$ type vertices, and vanishes on all the others. By inspection of the graph of flat states we find that the lattice of periodicities for the operator X, $\mathcal{R}_X$, is the span of $(1,0,-1)$, $(1,0,1)$, and $(0,1,0)$; these are the height difference vectors between the flat states in the support of X. This observation implies that $X[\mathbf{h}]$ can be expanded in a Fourier series over electric charges that live in the dual lattice $\mathcal{R}_x^*$ which is the span of $(\pi,0,\pi)$, $(\pi,0,-\pi)$, and $(0,2\pi,0)$.

If we consider the effect of S_X as a perturbation on the action of the FPL^2 model, the electric charges $(0,\pm 2\pi,0)$ play a special role. Namely, the operator product expansion of $\exp[i(0,2\pi,0)\cdot\mathbf{h}]$ and $\exp[-i(0,2\pi,0)\cdot\mathbf{h}]$ contains the $(\boldsymbol{\partial} h^2)^2$ operator, and therefore leads to the renormalization of K_{22} [25]. This follows from the fact that the background charge, Eq. (9), has a vanishing second component. On the other hand, for charges $\mathbf{e}$ with nonzero first or third component, the effect of the background charge is that the operator product expansion of $\exp(i\mathbf{e}\cdot\mathbf{h})$ and $\exp(-i\mathbf{e}\cdot\mathbf{h})$ does not contain $\boldsymbol{\partial} h^i \cdot \boldsymbol{\partial} h^j$ operators and therefore does not lead to the renormalization of the elastic constants K_{ij}.

The Coulomb gas representation of the height model provides a clear physical picture of the effect of S_X on the critical action of the FPL^2 model. For $w_X = 1$ the dimension of the $(0,\pm 2\pi,0)$ charges follows from Eq. (16),

$$x_X = \frac{(2\pi)^2}{4\pi K_{22}} = 2\left(\frac{1}{1-e_b} + \frac{1}{1-e_g}\right). \tag{14}$$

It is greater than 2 in the whole critical region of the FPL^2 model. These charges are therefore irrelevant in the renormalization group sense. In the Coulomb gas picture the $(0,\pm 2\pi,0)$ charges appear as bound pairs of neutral dipoles. Increasing w_X will have the effect of increasing the bare fugacity of these dipoles, which will in turn increase the value of the coupling K_{22} appearing in the effective field theory. Formally, this can be seen in perturbation theory making use of the operator product expansion [25]. Physically, the renormalization of K_{22} can be understood as the screening effect of dipoles. The dipoles lower the Coulomb energy between two electric test charges having a nonzero second component, corresponding to an increase in the value of K_{22} which plays the role of a dielectric constant.

At a critical value w_X^c there will be a Kosterlitz-Thouless-type transition of the SFL model into a flat state with a vanishing density of vertices at which the polymer bends. At the transition the $(0,\pm 2\pi,0)$ charges are marginal, i.e., their scaling dimension is equal to 2. Using Eq. (14) this observation gives rise to the prediction for the critical value of K_{22}:

$$K_{22}(w_X^c) = \frac{\pi}{2}. \tag{15}$$

For values of w_X smaller than w_X^c, K_{22} will be a *nonuniversal* function of w_X. In the $n_b = n_g = 1$ case, the formula K_{22}

$=\arcsin(w_X/2)$ follows from the exact solution of the 6V model [10]. The critical value of the vertex weight is $w_X^c(6V)=2$ and $K_{22}(2)=\pi/2$ is in agreement with Eq. (15). For other values of n_b and n_g our numerical transfer matrix calculations are in good agreement with Eq. (15).

The introduction of the vertex weight w_X also has an effect on the screening charges, Eq. (6), which appear in the Liouville part of the action. First consider the $n_b=n_g$ case of the SFL model. Due to the presence of the w_X term cyclic permutations of the four colors around a vertex are no longer a symmetry of the vertex weight. Therefore, unlike the $w_X=1$ case [17], there are now two independent elastic constants K_{22} and K_{11} appearing in S_E. $K_{13}=0$ follows from the remaining Z_2 symmetry of the vertex weights which are invariant under *two* cyclic permutations, such as $(\mathbf{A},\mathbf{B},\mathbf{C},\mathbf{D}) \rightarrow (\mathbf{C},\mathbf{D},\mathbf{A},\mathbf{B})$. The deduced structure of the elasticity matrix implies that the four electric charges in Eq. (6) are no longer degenerate in dimension for arbitrary w_X. Since the dimensions of $\mathbf{e}^{(1)}$ and $\mathbf{e}^{(2)}$ are independent of K_{22}, they are identified as the two screening charges tied to the nonrenormalizability of the loop weights [17]. As in the FPL^2 model we then assume that these two charges remain marginal when $n_b \neq n_g$. Using the dimension formula, Eq. (16), this then fixes the values of the two elastic constants, K_{11} and K_{13}, to the values quoted in Eq. (7).

Finally, it is interesting to look at some extreme limits of K_{22} in view of the effective field theory. Consider first the limit $K_{22}\rightarrow\infty$ in which height fluctuations in the second height component are completely suppressed. (As we are outside the critical phase, we are here referring to the bare value of the coupling.) Clearly, height fluctuations must always be present in the microscopic four-coloring model, but it is nevertheless instructive to look for the states that minimize the fluctuations of h^2. From the choice of the color vectors, Eq. (3), it is not difficult to see that on the four sites of $\{\mathbf{x}\}$ surrounding a given vertex, h^2 fluctuates by two units for the first four vertices of Fig. 3 and by one unit for the last two vertices. All vertices must therefore be of the c type, corresponding to the limit $w_X\rightarrow\infty$. Thus, $K_{22}\rightarrow\infty$ as $w_X\rightarrow\infty$.

Conversely, as $K_{22}\rightarrow 0$, the fluctuations in h^2 become unbounded and the effective field theory loses its consistency (since it was based on the assumption that the interfacial entropy is due to bounded fluctuations around the macroscopically flat states). However, the argument given above indicates that a small value of K_{22} should correspond to a small number of straight-going vertices in the loop model. Thus, we would conjecture that $K_{22}\rightarrow 0$ as $w_X\rightarrow 0$. This expectation is confirmed by the exact result for the 6V case [10] and also by extrapolation of our numerical results for $K_{22}(w_X)$ in the Flory case.

Apart from these limiting values, we would of course expect K_{22} to be a monotonically increasing function of w_X throughout the critical phase.

In the following section we compute the central charge and the scaling dimensions of various operators in the semiflexible loop model from its effective field theory. We identify quantities that depend on the nonuniversal elastic constant K_{22}; these are then predicted to vary continuously with w_X.

IV. OPERATORS AND SCALING DIMENSIONS

The effective field theory of the semiflexible loop model describes a Coulomb gas of electric and magnetic charges in the presence of background and screening charges. The magnetic charges $\mathbf{m}$ are vectors in $\mathcal{R}$ which is the lattice of periodicities of the graph of flat states, while the electric charges $\mathbf{e}$ take their values in the reciprocal lattice $\mathcal{R}^*$ [17]. With the normalization adopted for the vectors **A** through **D**, Eq. (3), $\mathcal{R}$ is a face-centered cubic lattice whose conventional cubic cell has sides of length 4, while $\mathcal{R}^*$ is a body-centered cubic lattice whose conventional cubic cell has sides of length π.

The scaling dimension of an operator which has total electromagnetic charge $(\mathbf{e},\mathbf{m})$ is the sum of its electric and magnetic dimensions, and it is a function of the elastic constants and the background charge [23]:

$$x(\mathbf{e},\mathbf{m}) = \frac{1}{4\pi}[(\mathbf{e}\mathbf{K}^{-1})\cdot(\mathbf{e}-2\mathbf{e}_0)+(\mathbf{m}\mathbf{K})\cdot\mathbf{m}]. \qquad (16)$$

$\mathbf{K}$ is the 3×3 matrix of elastic constants and $\mathbf{K}^{-1}$ is its inverse.

From Eq. (16) and the form of $\mathbf{K}$ [Eq. (5)] and $\mathbf{e}_0$ [Eq. (9)], it immediately follows that operators whose electric and magnetic charges both have a vanishing second component will have a K_{22}-independent scaling dimension. The scaling dimension in this case is independent of w_X and equal to its known value at $w_X=1$ [17]. Operators with $\mathbf{e}$ and $\mathbf{m}$ charges whose second components are not both zero will, on the other hand, have a scaling dimension that varies continuously with w_X. These predictions are confirmed by our numerical results.

A. Central charge

The central charge of the SFL model follows from its critical action. The three height components (bosonic free fields) each contribute one unit to the central charge while the contribution from the background charge is $12x(\mathbf{e}_0,0)$. Using Eq. (16) for $x(\mathbf{e}_0,0)$, Eq. (9) for the background charge $\mathbf{e}_0$, and the calculated values of the elastic constants K_{11} and K_{13}, Eq. (7), we find

$$c = 3 - 6\left(\frac{e_b^2}{1-e_b}+\frac{e_g^2}{1-e_g}\right), \qquad (17)$$

independent of the unknown value of K_{22}.

For the 6V model, which corresponds to the $e_b=e_g=1/3$ line in the SFL model, the above formula gives $c=1$ for the central charge along the critical line. This result also follows directly from the exact solution of the 6V model.

For the Flory model of polymer melting, which is the $e_b=1/2$, $e_g=1/3$ case, the predicted central charge is $c=-1$. This value is confirmed by our numerical transfer matrix calculations (see Sec. V).

B. Thermal operator

The SFL model can be thought of as the zero-temperature limit of a more general model where we allow for thermal

excitations that violate the fully packing constraint. Violations of the constraint lead to vertices with the four adjacent edges colored $(\mathbf{C},\mathbf{D},\mathbf{C},\mathbf{D})$. In the height representation such a vertex is identified with a topological defect (screw dislocation) whose charge, i.e., the sum of height differences around the vertex, is

$$\mathbf{m}_T = 2(\mathbf{C}+\mathbf{D}) = (0,-4,0). \tag{18}$$

Other vertices which have no **A** or **B** colored edges are possible, but they have a larger magnetic charge and are hence less relevant.

In the Coulomb gas picture a topological defect corresponds to a magnetic charge. Therefore, the thermal dimension can be calculated using Eq. (16), and we find

$$x_T = x(0,\mathbf{m}_T) = \frac{4}{\pi}K_{22}. \tag{19}$$

We make use of this equation below as it allows us to determine the unknown elastic constant K_{22} from a measurement of the thermal scaling dimension. Once this elastic constant is known, scaling dimensions of all electromagnetic operators can be calculated from Eq. (16).

C. String operators

A particularly important set of operators in any loop model are the string operators. Their two-point function is defined as the probability of having the small neighborhoods around two fixed points on the lattice, which are separated by a large distance, connected by s_b real loop segments and s_g ghost loop segments. For simplicity, we shall require s_b and s_g to be either both even or both odd; s_b+s_g odd requires L to be odd which produces a twist in the height, as discussed in Ref. [17]. In the height representation these string configurations are mapped to two topological defects, one serving as the source and the other as the sink of oriented loop segments. When the oriented loop segments wind around the defect points they are assigned spurious phase factors by the vertex weights; these phase factors can however be compensated by introducing appropriate electric charges at the positions of the defects [26].

In the case $s_b=2k_b$ and $s_g=2k_g$, i.e., when the number of real and ghost strings are both even, the electric and magnetic charge of the corresponding string operator are [17]

$$\mathbf{e}_{2k_b,2k_g} = -\frac{\pi}{2}(e_b,0,-e_b)(1-\delta_{k_b,0}) - \frac{\pi}{2}(e_g,0,e_g)(1-\delta_{k_g,0}),$$
$$\mathbf{m}_{2k_b,2k_g} = -2(k_b+k_g,0,k_g-k_b). \tag{20}$$

Since the charges have vanishing second component their dimension is independent of K_{22} and constant along the whole critical line $w_X \leqslant w_X^c$. The value of the string dimension follows from Eq. (16),

$$x_{2k_b,2k_g} = \frac{1}{2}\left[(1-e_b)k_b^2 + (1-e_g)k_g^2 - \frac{e_b^2}{1-e_b}(1-\delta_{k_b,0}) - \frac{e_g^2}{1-e_g}(1-\delta_{k_g,0})\right], \tag{21}$$

and is identical to that of the FPL^2 model [17]. Our numerical simulations confirm that even string dimensions are constant along the critical line.

In the odd string case, when $s_b=2k_b-1$ and $s_g=2k_g-1$, the electric and magnetic charge are [17]

$$\mathbf{e}_{2k_b-1,2k_g-1} = -\frac{\pi}{2}(e_g+e_b,0,e_g-e_b),$$
$$\mathbf{m}_{2k_b-1,2k_g-1} = -2(k_b+k_g-1,1,k_g-k_b). \tag{22}$$

Notably, the magnetic charge has a nonvanishing second component. Using Eq. (16) we calculate

$$x_{2k_b-1,2k_g-1} = \frac{K_{22}}{\pi} + \frac{1}{8}[(1-e_b)(2k_b-1)^2 + (1-e_g)(2k_g-1)^2] - \frac{1}{2}\left[\frac{e_b^2}{1-e_b} + \frac{e_g^2}{1-e_g}\right] \tag{23}$$

for the odd string dimension. It depends on the value of K_{22} and will therefore vary continuously with w_X. At the melting transition the exponents are exactly known from Eq. (15). This is confirmed by our numerical transfer matrix results, which we describe next.

V. TRANSFER MATRIX RESULTS

To check the correctness of our field theoretical predictions, we have numerically diagonalized the transfer matrix of the semiflexible loop model (and of its various generalizations, to be discussed below) defined on semi-infinite cylinders of even widths L ranging from 4 to 14.

The existence of a transfer matrix may not be *a priori* obvious, since the Boltzmann weights depend on the number of loops, which is a nonlocal quantity. We have however already shown in an earlier publication [17] how this is resolved by working in a basis of states that contains nonlocal information about how loop segments are interconnected at a given stage of the computations. In that paper, it was also shown that the full transfer matrix contains various sectors, the leading eigenvalues of which provide finite-size estimations of the free energy and of the various critical exponents, using the standard conformal field theory (CFT) relations [27,28]

$$f_0(L) = f_0(\infty) - \frac{\pi c}{6L^2} + \cdots, \tag{24}$$

$$f_k(L) - f_0(L) = \frac{2\pi x_k}{L^2} + \cdots. \tag{25}$$

Here, the label k refers either to a higher eigenvalue in the sector to which f_0 belongs, or to the leading eigenvalue in

another sector characterized by some topological defect of charge k.

To access critical exponents, we shall mainly be concerned with topological defects that consist in enforcing that a certain number of strings of either flavor propagate along the length direction of the cylinder. These give rise to a two-parameter family of critical exponents x_{s_b,s_g} corresponding to s_b real strings and s_g ghost strings. The corresponding topological charges, Eqs. (20) and (22), take the form of three-dimensional electromagnetic vector charges. In the transfer matrix calculations, each of these topological sectors is associated with a different state space. The difficulty of precisely characterizing these spaces limited our previous approach [17] to at most two strings. In the Appendix we present an algorithm that explicitly constructs the required state spaces for any (s_b,s_g), based on an iterative procedure and hashing techniques.

By inspection of the eigenstates produced by our previous algorithm [17], it turns out that many of the basis states carry zero weight. One would then expect that identical results can be obtained more efficiently by working in a basis in which such states have been eliminated from the outset. We defer the technical details of how this can be done to the Appendix. It is also shown how the block-diagonalization scheme can be carried even further, by exploiting various conservation laws that are most easily understood from the analogy between the SFL model and the six-vertex model. One important consequence is that the constrained free energy $f_T(L)$ that is linked to the thermal scaling dimension can now be obtained as a leading eigenvalue, rather than as the second eigenvalue in the stringless sector. This considerably improves the efficiency of the computations.

Finally, the matrix elements need some modification in order to take into account the bending rigidity parameter w_X. This is readily done, without any modification of the basis states, since w_X is a purely local quantity.

Before turning to our numerical results, we should mention that we have submitted our transfer matrices to several tests, in order to verify their correctness:

(1) For $w_X=1$, all numerically determined string dimensions x_{s_b,s_g} with $s_b+s_g=2$ or 4 agree to at least three significant digits with their exact values in the cases $(n_b,n_g)=(1,1)$ [10] and $(n_b,n_g)=(0,1)$ [17].

(2) All eigenvalues found for the FPL^2 model agree with those obtained from our previous algorithm [17].

(3) For the six-vertex model [10], we have compared the extrapolated bulk free energy with Baxter's exact expression.

(4) Again for the six-vertex model, we find excellent agreement with the exact formulas $x_{1,1}=K_{22}/\pi$ and $x_T=4K_{22}/\pi$, where $K_{22}=\arcsin(w_X/2)$ is the elastic constant.

(5) We have also found agreement with the first few terms in diagrammatic expansions around various limits of infinite fugacities.

A. Central charge

A crucial prediction of our field theory is that, for given values of the loop fugacities (n_b,n_g), the central charge of the SFL model should be independent of w_X, as long as the latter is constrained to the critical regime, $0<w_X\leqslant w_X^c$.

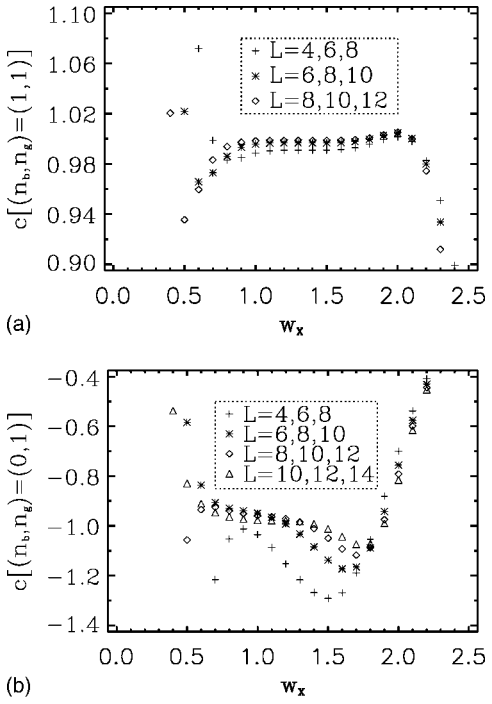

FIG. 4. Central charge c as a function of the bending rigidity w_X for the 6V model (left) and the semiflexible loop model (right). We show three-point fits for different system sizes, as indicated.

In Fig. 4 we show the effective central charge as a function of w_X, in the cases $(n_b,n_g)=(1,1)$ and $(0,1)$. The result $c=1$ for $0<w_X\leqslant 2$ is well established for the 6V model, but the plot for this case is still useful as it gives us some guidance as to what finite-size effects to expect. In particular, note that these become more pronounced when w_X is small, and that the termination of critical behavior at $w_X=2$ is clearly signaled by the finite-size data leveling off. Another effect is that while for $w_X<2$ the distance between successive estimates decreases with system size, for $w_X>2$ we observe this distance to increase.

Although finite-size effects play a more important role in the $(n_b,n_g)=(0,1)$ case, the general picture is quite similar. The figure leaves little doubt that $c=-1$ for $0<w_X\leqslant w_X^c$. We also obtain a first rough estimate $w_X^c=1.95\pm0.15$, not far away from the 6V-model value.

Here, and elsewhere, we mainly show fits in which the convergence of Eqs. (24) and (25) has been accelerated through the inclusion of a nonuniversal $1/L^4$ correction, as predicted by conformal invariance.

B. String dimensions

We next turn to the computation of the magnetic-type scaling dimensions x_{s_b,s_g} describing the scaling of the operator that inserts s_b real strings and s_g ghost strings. To study these, the width L of the strip must have the same parity as s_b+s_g. For simplicity we shall limit ourselves to the case of even L. There are then two classes of exponents: Those in which s_b and s_g are both even, and those in which they are

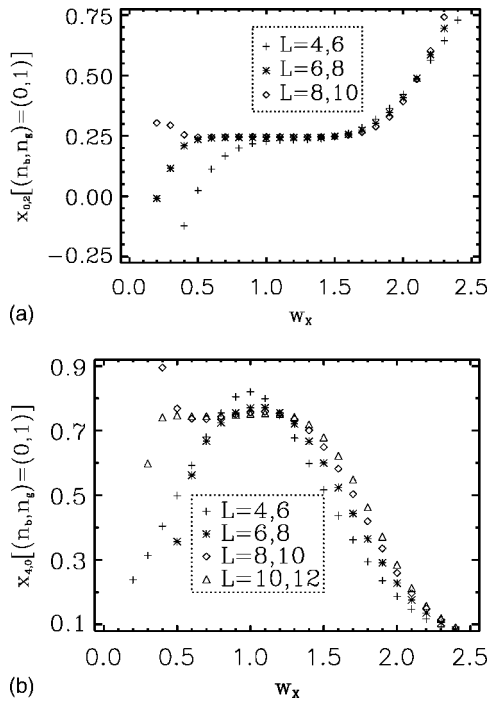

FIG. 5. Scaling dimensions x_{s_b,s_g} with even s_b and s_g. The left and right panels show, respectively, $x_{0,2}$ and $x_{4,0}$. System sizes used in the two-point fits are also indicated.

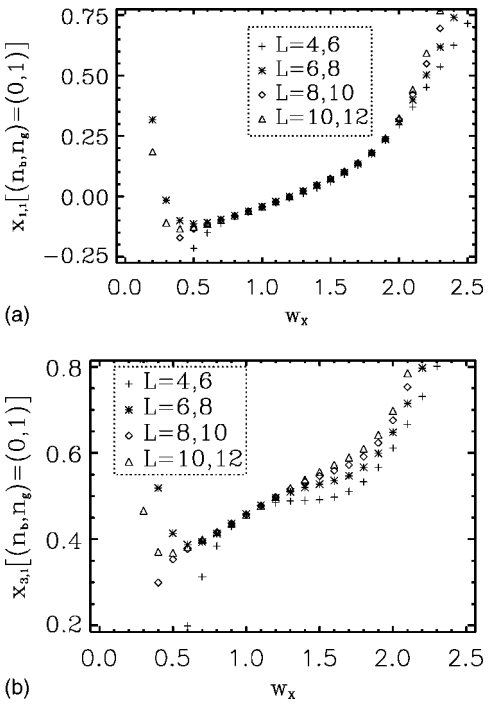

FIG. 6. Scaling dimensions x_{s_b,s_g} with odd s_b and s_g. We show $x_{1,1}$ (left) and $x_{3,1}$ (right) for the SFL model.

both odd. The field theory predicts that the former should stay constant on the critical line, parametrized by w_X, while the latter are expected to vary continuously as functions of w_X; see Sec. IV C.

On Fig. 5 we show two examples of exponents with s_b, s_g even, within the SFL model $[(n_b,n_g)=(0,1)]$ with varying w_X. They correspond, respectively, to the insertion of two ghost strings ($x_{0,2}$) and of four real strings ($x_{4,0}$). From the figure it should be evident that $x_{0,2}=\frac{1}{4}$ and $x_{4,0}=\frac{3}{4}$ are constant throughout the critical phase. In the latter case the finite-size variations are quite pronounced, as might have been anticipated given the higher number of strings. Careful observation of the distance between subsequent finite-size points however strongly suggests that the variation will eventually die away.

Examples of exponents with s_b, s_g odd are given in Fig. 6. In both cases, $x_{1,1}$ and $x_{3,1}$, the convergence to monotonically increasing functions of w_X is clearly brought out. Also note the agreement with the exact results for $w_X=1$, which read $x_{1,1}=-\frac{5}{112}\simeq -0.0446$ and $x_{3,1}=\frac{51}{112}\simeq 0.455$ [17], respectively.

C. Thermal scaling dimension

As described in the Appendix, the thermal scaling dimension is linked to the gap between transfer matrix sectors in which there is an even (respectively an odd) number of flavor crossings in the basis states. Because of the relation

$$K_{22}=\frac{\pi}{4}x_T, \tag{26}$$

measuring this gap gives a direct means of accessing the elastic constant associated with the second height component in the field theory.

According to the field theory, K_{22} is a nonuniversal function of w_X, and once it is known the values of all the other critical exponents follow. This suggests the following numerical check of the field theoretic scenario. For several values of w_X, we measure x_T from the transfer matrix, and use it to determine K_{22}. We then compute the predictions for the various other scaling dimensions (the x_{s_b,s_g}) from the field theory, Eq. (16), by use of the numerically determined value of K_{22}, and compare them with values measured directly from the transfer matrices.

The result of this verification is shown in Table I. The values for x_T are based on transfer matrices for strips up to size $L=14$, here extrapolated to the limit $L\to\infty$. The agreement between the CFT predictions and numerics is in general excellent. Note, however, that the precision deteriorates whenever w_X approaches zero or w_X^c, effects which are also clearly visible in Figs. 4–6.

The origin of these numerical shortcomings can be understood from the field theory. First, for $w_X\to 0$ we have $K_{22}\to 0$ and the fluctuations in the second height component become unbounded. Microscopically, the dominant configurations are those of long strands of wiggling lines ("helices") whose persistence length increases with decreasing w_X. Strong corrections to scaling will set in when this length becomes comparable to the system size L. Second, for $w_X\to w_X^c$ we are approaching a Kosterlitz-Thouless-type phase transition, and strong logarithmic corrections to scaling are expected due to the marginality of the operator T.

Based on the data in Table I, we can refine our estimate for the location of the melting transition:

$$w_X^c=1.92\pm 0.02. \tag{27}$$

In Fig. 7 we compare our numerical results for the curve $x_T(w_X)$ in the SFL case with the exactly known result of the

TABLE I. Thermal exponent x_T measured for varying values of w_X. The corresponding values of the scaling dimensions $x_{1,1}$, $x_{3,1}$, and $x_{1,3}$ as predicted by our conformal field theory (column marked CFT) are compared with their numerically measured counterparts (column marked Num.).

w_X	x_T	$x_{1,1}$		$x_{3,1}$		$x_{1,3}$	
		CFT	Num.	CFT	Num.	CFT	Num.
0.4	0.141(7)						
0.5	0.207(5)						
0.6	0.275(4)	−0.117	−0.115	0.383	0.385	0.549	0.548
0.7	0.346(3)	−0.100	−0.100	0.400	0.402	0.567	0.565
0.8	0.413(2)	−0.087	−0.085	0.413	0.418	0.580	0.582
0.9	0.4913(7)	−0.065	−0.066	0.435	0.436	0.601	0.601
1	$\frac{4}{7}$	$-\frac{5}{112}$		$\frac{51}{112}$		$\frac{209}{336}$	
1.1	0.6525(10)	−0.026	−0.025	0.474	0.475	0.641	0.643
1.2	0.7429(5)	−0.002	−0.002	0.498	0.498	0.665	0.665
1.3	0.8365(3)	0.022	0.022	0.522	0.521	0.688	0.688
1.4	0.9374(1)	0.047	0.048	0.547	0.546	0.713	0.715
1.5	1.0490(1)	0.075	0.076	0.575	0.576	0.742	0.75
1.6	1.1769(7)	0.107	0.11	0.607	0.62	0.774	0.80
1.7	1.333(2)	0.148	0.15	0.648	0.68	0.815	0.90
1.8	1.541(5)	0.202	0.20	0.702	0.7	0.869	0.9
1.9	1.861(8)	0.29	0.3	0.79	0.8	0.95	1.0
w_X^c	2	$\frac{5}{16}$		$\frac{13}{16}$		$\frac{47}{48}$	

6V model, $x_T=(4/\pi)\arcsin(w_X/2)$ [10]. Although the functional forms are quite reminiscent, we have unfortunately not been able to conjecture a convincing exact expression in the SFL case.

VI. PHASE DIAGRAM

A. Generalized six-vertex model

Given the one-to-one correspondence between the six vertex configurations in the FPL^2 model and the six arrow configurations in the six-vertex model (see Fig. 3), it is natural to define a generalized six-vertex model in which the standard arrow weights are supplemented by the nonlocal loop weights n_b, n_g of the FPL^2 model.

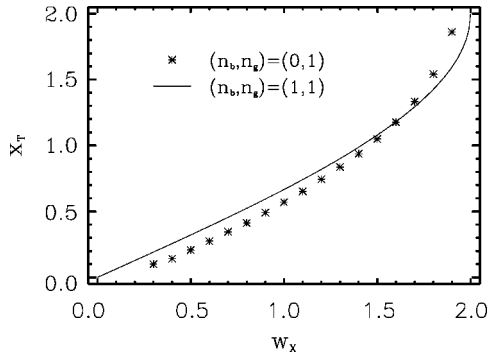

FIG. 7. Thermal scaling dimension x_T versus bending rigidity w_X in the Flory model (symbols), as compared to the exact result of the six-vertex model (line).

Until now we have only considered the isotropic case of $a=b$. (See Fig. 3. Let us briefly recall the effect of taking $a\neq b$ in the six-vertex model [10]. Define the parameters w and μ by

$$\Delta=\frac{a^2+b^2-w_X^2}{2ab}=-\cos\,\mu,\quad 0<\mu<\pi, \tag{28}$$

$$\frac{a}{b}=\frac{\exp(i\mu)-\exp(iw)}{\exp(i\mu+iw)-1},\quad -\mu<w<\mu. \tag{29}$$

Then, taking $a\neq b$ corresponds to twisting the usual square lattice into a rhombus, defined by the anisotropy angle [29]

$$\theta=\frac{\pi}{2}\left(1+\frac{w}{\mu}\right). \tag{30}$$

All this means is that the central charge and the critical exponents, when measured in the usual way from a transfer matrix, get multiplied by a geometrical factor of $\sin(\theta)$.

In Fig. 8 we plot the effective central charge of the SFL model with $b=w_X=1$ and varying a against the variable $\tau=\theta/\pi$, defined in terms of the above 6V expressions. By the word "effective" we mean that we do not correct for the lattice distortion, the effect of which can then be read off from the graph. If the effect of the anisotropy were the same as in the 6V model, the plot should just look like the function $-\sin(\pi\tau)$, since the SFL model has (real) central charge $c=-1$. Clearly, this is not the case, and so the nonlocality of the loop weights has a nontrivial effect on the anisotropy factor. We leave this as an interesting open question.

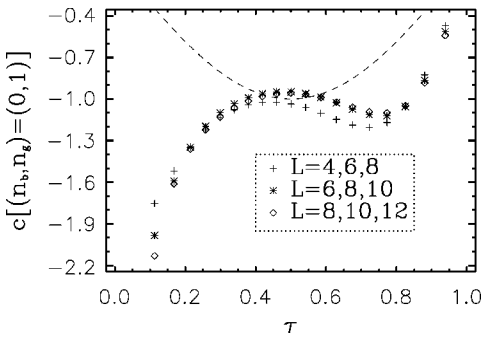

FIG. 8. Anisotropy effects in the generalized six-vertex model with $(n_b,n_g)=(0,1)$. The symbols show the effective central charge for various system sizes. For comparison, the dashed line shows the function $-\sin(\pi\tau)$, which would have been the exact result if the anisotropy had the same effect as in the six-vertex model.

B. Generalized eight-vertex model

It is also of interest to consider the loop generalization of the eight-vertex model. In terms of the loops there are two different ways of resolving the vertices that act as sources or sinks of the eight-vertex arrows, and so we are led to consider the ten-vertex model defined by Fig. 9. In addition to the local weights which are shown on the figure, we assign the usual nonlocal loop weights n_b and n_g.

For simplicity, we shall disregard the effects of anisotropy, and thus only two types of local weights are of interest. The first is the weight w_X of having the two loop flavors cross, same as in the SFL model. The second is a contact interaction w_c, assigned to the vertices where two loop segments of the same flavor touch one another. One may consider letting it depend on the flavor index, but in order to stay close to the definition of the conventional eight-vertex model we shall here take the contact interaction to be flavor independent.

The motivation for the contact interaction is to be able to exclude the loops of a given flavor from any number of lattice vertices. As this violates the compactness constraint, we expect the conclusions of our earlier paper on the transition from the compact to the dense phase [30] to apply. A nonzero value of w_c should induce a flow towards a phase where the two loop flavors decouple, and the critical properties are just those of two noninteracting $O(n)$ models (with $n=n_b$ and n_g respectively) in the low-temperature (dense) phase.

A detailed numerical study of the behavior of the effective central charge in the parameter space (w_X,w_c) has led us to suggest that the phase diagram of the generalized eight-vertex model is as shown on Fig. 10.

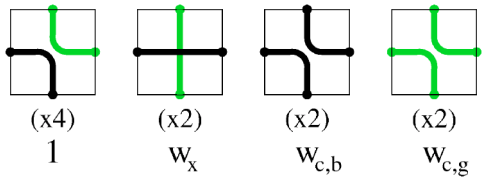

FIG. 9. Vertices defining the generalized eight-vertex model, along with their corresponding multiplicities and local weights.

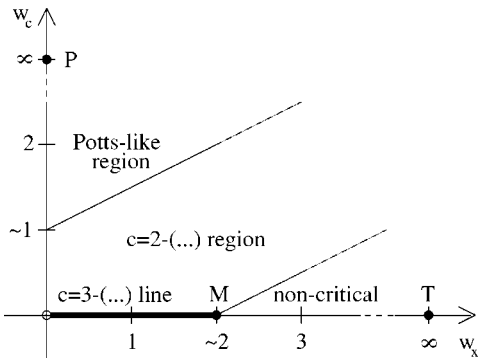

FIG. 10. Proposed phase diagram of the generalized eight-vertex model.

For $w_c=0$, the model reduces to the SFL model, and so below the melting point M (i.e., for $w_X<w_X^c$ with, very roughly, $w_X^c\approx 2$) we have a line of critical points along which critical exponents that depend on the second height component vary continuously, while the central charge

$$c(n_b,n_g)=3-\frac{6e_b^2}{1-e_b}-\frac{6e_g^2}{1-e_g} \tag{31}$$

is constant. The end point of the SFL line, with $w_X=\infty$, is a trivial attractive fixed point T, favoring configurations in which all loops go straight in the bulk (they are necessarily reflected at the boundaries enjoying free boundary conditions). The point T is believed to govern the theories to the right of M (i.e., with $w_X>w_X^c$), including a portion of the phase diagram with nonzero but small w_c (see Fig. 10).

Moving away from the critical line of the SFL model, towards positive values of the contact interaction, we observe numerically that the central charge drops abruptly by one unit, and stays constant as a function of w_c up to some finite critical value w_c^c that depends on w_X. This is the dense phase of the DPL^2 model [30] with central charge

$$c(n_b,n_g)=\left(1-\frac{6e_b^2}{1-e_b}\right)+\left(1-\frac{6e_g^2}{1-e_g}\right). \tag{32}$$

Here, the two loop-flavors decouple, and critical exponents are just the sum of the critical exponents for two noninteracting $O(n)$ models (with $n=n_b$ and n_g) in the dense phase. We have verified numerically this prediction for the exponent $x_{1,1}$ for a number of different loop fugacities. We have also observed numerically that the critical exponents do not depend on w_X throughout the dense phase. This confirms the expectations that in noncompact phases the only effect of the bending rigidity is to renormalize the persistence length of the polymer, as already discussed in the Introduction.

Finally, for w_c large enough, the numerically evaluated central charges suggest that the models flow into an attractive fixed point P situated at $(w_X,w_c)=(0,\infty)$. Here, only contact-type vertices are allowed, and since the different loop flavors can no longer coexist, the partition function at P becomes simply a sum, $Z=Z_b+Z_g$, where Z_k involves only contact vertices of flavor k (with $k=b,g$). But clearly Z_k is just the loop-model representation [10] of a self-dual Potts

model with $q_k=(n_k)^2$ states. It is intuitively clear (and explicitly brought out by the exact solution [10]) that the free energy of the q-state Potts model is an increasing function of q. Therefore, the sum $Z=Z_b+Z_g$ will be dominated by the term with the largest value of q. Thus, the point P has central charge

$$c(n_b,n_g)=\max\left(1-\frac{6e_b^2}{1-e_b},1-\frac{6e_g^2}{1-e_g}\right), \tag{33}$$

and, by the usual identification of the critical Potts model with the dense phase of the $O(n=\sqrt{q})$ model, the critical exponents are simply those of a single $O[\max(n_b,n_g)]$ model in the dense phase.

We would expect that only this large-w_c portion of the phase diagram gets modified by letting the contact interaction be flavor dependent. Let us recall that in the conventional $O(n)$ model [2] with a finite *positive* vacancy fugacity w_c the critical behavior of the loops is described by either of *two* critical branches. The first branch, known as the *dense* branch [2,31], is attractive in w_c and as such controls the entire domain of low w_c. Its central charge is the one referred to above:

$$c=1-6\tilde{e}^2/(1-\tilde{e}) \tag{34}$$

in the usual parametrization $n=2\cos(\pi\tilde{e})$. The second branch, known as the *dilute* branch [2,32], is repulsive in w_c and as such requires w_c to be tuned to a particular n-dependent critical value. In other words, the fugacity of a vacancy can tune the $O(n)$ model to its critical point. The central charge of the dilute phase is

$$c=1-6\tilde{e}^2/(1+\tilde{e}), \tag{35}$$

using the same parametrization as above.

In particular, in the DPL^2 model [30] the two loop-flavors act as decoupled $O(n)$ models, and depending on the fugacities of the two flavors of vacancies each of the models can reside in either the dense or the dilute phase, giving a total of four different phases. We expect this conclusion to hold true in the generalized eight-vertex model (i.e., with an added bending rigidity w_X). Note that only when $n_b=n_g$ can we simultaneously take the two $O(n)$ models to their critical point by tuning a vacancy fugacity w_c which is common for the two loop-flavors. In the general case, when $n_b\neq n_g$ we would need two distinct parameters, $w_{c,b}$ and $w_{c,g}$, as indicated on Fig. 9. Presumably, this would lead to a richer phase diagram, with critical lines corresponding to dense-dilute, dilute-dense, and dilute-dilute behavior of the two $O(n)$ models.

Let us return to the phase diagram shown in Fig. 10. In the special case of the eight-vertex model, the two oblique transition lines shown on Fig. 10 are known to be of slope $1/2$ [10]. Actually, they are just images of the line OM under certain exact symmetries of the eight-vertex model [10]. Thus, they have again $c=1$, whereas the "bulk" of the phase diagram is noncritical.

These two features can be accounted for within the framework of the generalized eight-vertex model with $(n_b,n_g)=(1,1)$. First, note that our field theory predicts that the region on Fig. 10 which is limited by the two oblique lines and the coordinate axes is actually *critical* with central charge $c=0$ (dense phase); this is obtained by setting $e_b=e_g=1/3$ in Eq. (32). This is not in contradiction with the exact result [10] that this same region is noncritical within the eight-vertex model. Namely, the generalized eight-vertex model is embedded in a much larger Hilbert space. More precisely, our statement is that the first and third height components possess critical fluctuations and constitute a $c=0$ theory, even though the second height component is massive. This scenario is brought out very clearly by the numerics, as we observe the leading transfer matrix eigenvalues in the sectors determining the free energy and x_T to *coincide* within the concerned region. Thus, x_T and K_{22} vanish identically, cf. Eq. (26).

Second, the field theory also accounts for the fact that, within the 8V model, the two oblique lines are critical with $c=1$. Namely, we claim that they simply correspond to dilute-phase behavior within the generalized 8V model. More precisely, since $n_b=n_g$, the two decoupled $O(n)$ models must be driven to their critical points simultaneously by tuning the common parameter $w_{c,b}=w_{c,g}\equiv w_c$. Setting $\tilde{e}=1/3$ in Eq. (35) gives a contribution of $c=1/2$ for each of the models, whence $c_{\text{total}}=1/2+1/2=1$ as expected.

Finally, in the 8V model, the part of the w_c axis with $0<w_c<1$ constitutes a further image of the line OM under an exact symmetry. We believe this to be "accidental" in the sense that we have seen no sign of a finite interval of the w_c being critical within the generalized 8V model with other values of the fugacities.

Taking a common contact parameter $w_{c,b}=w_{c,g}$ for the generalized 8V model with $n_b\neq n_g$ destroys the criticality of the two oblique lines of Fig. 10. They still act as transition lines in the sense that they separate the basins of attraction of the dense phase and the points P and T, respectively. However, the transition is now expected to be a first-order one. This is confirmed by our numerical results for the $(n_b,n_g)=(0,1)$ case which show that the effective central charge develops violent finite-size effects upon approach of the transition lines. Further support for this scenario is furnished by Monte Carlo simulations [12] where a finite concentration of empty sites was shown to lead to a first-order transition.

The oblique lines in Fig. 10 are expected to move away from their exactly known 8V positions when we vary the loop fugacities away from the trivial values $(n_b=n_g=1)$. Some evidence for this is already available from our determination of the melting point M in the Flory case; see Eq. (27). In general, we have been able to numerically determine the position of the uppermost line from the transfer matrix spectra. Recall from the discussion near Eq. (26) that the coupling K_{22} can be linked to the gap between the leading eigenvalues in two topologically characterized transfer matrix sectors. By scanning through w_c at fixed w_X we have observed (at least in the Flory case) that these two eigenvalues become degenerate as soon as w_c moves away from zero (even at a value as small as $w_c\simeq 10^{-6}$). This degeneracy

eventually disappears when there is a level crossing in the ground-state sector of the transfer matrix, at some finite w_c.

We have measured the position of this level crossing as a function of system size and extrapolated it to the thermodynamic limit. To test the reliability of the method, we have first applied it to the $(n_b,n_g)=(1,1)$ case. Our final estimate $w_c=1.52\pm0.02$ at fixed $w_X=1$ is in good agreement with the exact result $w_c=3/2$ [10]. The same method applied to the Flory case, $(n_b,n_g)=(0,1)$, yields $w_c=1.4294\pm0.0005$ at $w_X=1$ and $w_c=1.958\pm0.005$ at $w_X=2$. These values are clearly different from those predicted by the 8V model.

In conclusion, we believe that it would be most interesting to study the generalized eight-vertex model in more detail, using the exact techniques of integrable systems. In particular, it is conceivable that the present treatment misses some subtle exceptional points in the phase diagram.

VII. DISCUSSION

The semiflexible loop model was defined as a generalization of the two-flavor fully packed loop model on the square lattice, by introducing a vertex weight associated with vertices at which the loop does not undergo a 90° turn. We have proposed an effective field theory of the semiflexible loop model based on its height representation. This leads to exact results for the Flory model of polymer melting in two dimensions. Furthermore, we have shown that the loop model provides a generalization of the eight-vertex model with an interesting phase diagram. Here we comment further on these two main results.

A. Scaling of semiflexible compact polymers

Polymers configurations are random, and as such, they are described by probability distributions. Their critical nature, in the long-chain limit, is revealed by the fact that these distributions have scaling forms characterized by universal exponents. The simplest distribution is the probability $p(r,l)$ that the end-to-end distance equals r for a polymer of contour length l. In the scaling limit, when r is much greater than the lattice spacing and much less than the radius of gyration of the polymer, we have [1]

$$p(r,l) = r^{\theta} f(r/l^{\nu}). \tag{36}$$

Here f is a scaling function, ν is the "swelling exponent," and θ the "cyclization exponent."

For semiflexible compact polymers, which correspond to the Flory model with $w_X \leqslant w_X^c$, the swelling exponent is $\nu=1/2$. This is an exact result which simply follows from the fact that compact polymers are space filling, regardless of w_X. Furthermore, the swelling exponent can be related to the string dimension $x_{2,0}$ through the scaling law $\nu=(2-x_{2,0})^{-1}$ [16]. Then replacing $e_b=1/2$ and $e_g=1/3$ in Eq. (21) gives $x_{2,0}=0$ and $\nu=1/2$, for all values of w_X. This calculation then serves as a nontrivial check on the field theory.

The cyclization exponent is related to the scaling dimension associated with one real and one ghost loop segment: $\theta=-2x_{1,1}$ [17]. From Eq. (23) it follows that θ will vary continuously as the polymer is made stiffer by increasing w_X. At the melting transition the exact result for θ follows from the computed value of the critical elastic constant, Eq. (15),

$$\theta^c = -\tfrac{5}{8}. \tag{37}$$

The negative value implies that at the transition (and slightly below it) the two ends of the polymer feel an effective *attraction*. This is surprising as the naive expectation is that the two ends of a polymer will feel an effective repulsion due to the self-avoiding constraint. For stiff compact polymers this naive expectation is not met. Whether this will persist in three dimensions is an interesting open question.

B. Generalized eight-vertex model

The generalized 8V model gives a quite detailed modelization of two-dimensional lattice polymers. It possesses the following features.

(a) Steric constraints (self-avoidance and connectedness of the polymer chains) are modeled exactly.

(b) Possibility of introducing polydispersity, by taking n_b away from zero.

(c) A bending rigidity parameter w_X allows to control the transition between a melt and a crystalline phase.

(d) A contact interaction parameter w_c (or alternatively, a fugacity of a vacancy) controls the transitions between compact, dense, dilute, Potts-like, and noncritical phases.

(e) Possibility of introducing nonlocal interactions (although of a peculiar form), by taking n_g away from one.

The phase diagram of a somewhat similar model was studied in the Bethe approximation by Lise, Maritan, and Pelizzola [33]. However, in the compact limit the results of these authors are equivalent to Flory's mean-field treatment, as they do not take into account the nonlocal features of the polymers. We have here treated the excluded-volume effects in an exact manner. On the other hand, the model of Ref. [33] includes an additional feature.

(f) A contact interaction between nonconsecutive monomers that are nearest neighbors on the lattice allows to drive the model to tricriticality, i.e., to access the θ-point physics.

This interaction is not present in the generalized 8V model. If we were to include it, we would need the contact interaction to be flavor dependent (the authors of Ref. [33] do not consider what we refer to as ghost loops). However, we do not believe that anything new can be learnt from such a generalization. First, the contact interaction is redundant in the compact phase ($w_c=0$), as the number of contacts is constant (actually maximal) in any fully packed configuration. Second, in the noncompact phases ($w_c\neq0$) our field theory predicts a decoupling into two independent $O(n)$ models. One would expect the flavor-dependent contact interactions to act independently on the two decoupled models, and the problem essentially reduces to that of the θ-point physics of a standard $O(n)$ model [34].

We leave it as an interesting question whether the generalized 8V model can be tackled using the methods of integrable systems. From Fig. 9 it can obviously be formulated as a 40-vertex model (taking into account the loop orienta-

tions) with complex vertex weights. To our knowledge, such a model has not been studied previously. If one could solve it, it would be particularly interesting to work out the exact expression of the coupling constant $K_{22}(w_X)$ as a function of the loop fugacities n_b and n_g. Also, it is conceivable that our field theoretical approach has missed some exceptional critical points in the phase diagram.

C. Order of the melting transition

In this paper we have established that the order of the melting transition within the Flory model is second order, as first suggested by Saleur [13]. We have also explained how the introduction of a finite density of vacancies may lead to a first-order transition, as observed in Monte Carlo simulations [12]. This combined scenario settles a long controversy in the literature [8].

ACKNOWLEDGMENTS

We are grateful to Ken Dill for introducing us to the Flory model of polymer melting. J.K. would further like to thank the KITP in Santa Barbara for hospitality, where this work was initiated. The research of J.K. was supported by the NSF under Grant No. DMR-9984471 and by the Cottrell Foundation.

APPENDIX: CONSTRUCTION OF THE TRANSFER MATRICES

The transfer matrix construction of Ref. [17] relied on an explicit bijection between the set of allowed connectivity states $\mathcal{C}$ and the set of integers $Z_{|\mathcal{C}|}=\{1,2,3,\ldots,|\mathcal{C}|\}$. However, in many cases it is difficult to furnish an *a priori* characterization of the set of allowed basis states and its cardinality. Moreover, some of the states utilized in Ref. [17] were found to carry zero weight in the leading eigenvectors of the corresponding sectors of the transfer matrix, and so one should think that it would be possible to eliminate them from the outset.

To remedy this situation it is preferable to use another approach. Without prior knowledge of the state space, the latter is explicitly generated by acting with the transfer matrix $\mathcal{T}$ on a reference state $|v_0\rangle$ which is known to belong to the image of $\mathcal{T}$ in the concerned sector. In this way, a certain number of image states is generated, which can be inserted in an appropriate data structure using hashing techniques [35]. One then acts with $\mathcal{T}$ on these states, generating a new list of states, and continues in this way until no new states are generated. The resulting list is the complete state space of $\mathcal{T}$ in the concerned sector.

It remains to find an appropriate reference state $|v_0\rangle$ for each physically interesting sector of $\mathcal{T}$. For the sector (s_b,s_g) in which s_k flavor-k strings ($k=b,g$) span the length of the cylinder generated upon action of $\mathcal{T}$, the reference state can be chosen as shown in Fig. 11. This state simply consists of $(L-s_b-s_g)/2$ real arches followed by s_b real strings and s_g ghost strings. L must of course have the same parity as s_b+s_g.

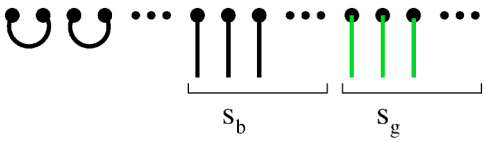

FIG. 11. Reference state used for generating the sector with s_k flavor-k strings ($k=b,g$).

Choosing the sector corresponding to the thermal scaling dimension is a little less obvious. A useful observation is made by exploiting the correspondence with states of the six-vertex model, as depicted in Fig. 3. In a given row, let N_k^{even} and N_k^{odd} be the number of flavor-k loop segments residing on even and odd vertical edges, respectively. Then define

$$Q=(N_b^{\text{even}}-N_b^{\text{odd}})-(N_g^{\text{even}}-N_g^{\text{odd}}). \tag{A1}$$

By inspection of Fig. 3 it is seen that Q is nothing but the vertical flux of arrows within a given row. By the ice rule, Q is a conserved quantity and can thus be used to label a sector of $\mathcal{T}$.

The reference state of Fig. 11 with $(s_b,s_g)=(0,0)$ is seen to have $Q=0$. The first excited state with no strings has $Q=\pm 4$ and is depicted in Fig. 12. Its first four sites are occupied by mutually penetrating real and ghost arches, followed by $(L-4)/2$ simple real arches. In general, for any given L, states with $Q=\pm 4q$ exist for $q=0,1,\ldots,\lfloor L/4\rfloor$. The number of states in the kth sector is just

$$\sum_{n=q}^{L/2-q}\binom{L/2}{n+q}\binom{L/2}{n-q}C_{L/2-n}C_n, \tag{A2}$$

where $C_n=(2n)!/n!(n+1)!$ are the Catalan numbers. Using a sum rule on the binomial coefficients, it is easily seen that the total number of states without strings, summed over the sector index q, reads simply

$$\sum_{n=0}^{L/2}\binom{L}{2n}C_{L/2-n}C_n. \tag{A3}$$

This is nothing but the dimension of the state space used in Ref. [17].

From entropic reasons it is fairly obvious that the free energy belongs to the sector $q=0$. We are now going to argue that the thermal scaling exponent is linked to the gap between the first eigenvalue in the $q=0$ and $q=1$ sectors, cf. Eq. (25). The first reason is that, by construction, the $q=1$ constraint acts as an excitation within the full state space [with all values of q included, as in Eq. (A3)], and hence should correspond to a subdominant eigenvalue within that space. Indeed, it is observed numerically that the second eigenvalue obtained from the transfer matrix of Ref. [17] co-

FIG. 12. Reference state used for generating the thermal sector.

TABLE II. Sizes of various sectors of the SFL model transfer matrix defined on a cylinder of width L with periodic boundary conditions. The symbol (s_b,s_g) labels the sector in which s_k flavor-k strings ($k=b,g$) run along the length of the cylinder. The sectors $(0,0)$ and "Thermal" have no strings, but the parity of the number of flavor crossings in the basis states is fixed to be even and odd, respectively.

L	$(0,0)$	Thermal	$(2,0)$	$(1,1)$	$(4,0)$	$(3,1)$	$(2,2)$
2	2		1	1			
4	8	1	8	12	1	2	2
6	46	12	69	141	15	42	72
8	332	124	664	1720	196	684	1056
10	2784	1280	6960	21760	2520	10320	14800
12	25888	13605	77664	283584	32565	151500	205920
14	259382	149604	907837		425019		

incides with the leading eigenvalue of the $q=1$ sector, obtained by using the techniques outlined above.

As a second argument, note that in the language of the SFL model height mapping, encircling the first four sites of Fig. 12 yields a height dislocation of $\mathbf{A}-\mathbf{C}+\mathbf{B}-\mathbf{D}$. By the four-coloring rule, $\mathbf{A}+\mathbf{B}+\mathbf{C}+\mathbf{D}=\mathbf{0}$, this is the same as

$$\mathbf{m}_T = 2(\mathbf{A}+\mathbf{B}) = -2(\mathbf{C}+\mathbf{D}). \tag{A4}$$

But the latter is *also* the height defect associated with a defect vertex $(\mathbf{C},\mathbf{D},\mathbf{C},\mathbf{D})$ that corresponds to excluding the real loops from that vertex, which is exactly a thermal-type excitation (and to wit the one that is used for computing the critical exponent x_T within the field theory).

In the field theory, one might compute the exponent corresponding to the insertion of magnetic defects $\pm q'\mathbf{m}_T$ at either end of the cylinder. In the transfer matrix, these should simply be linked to the gap between the sectors $q=0$ and $q=q'$.

In Table II we show the sizes of the various transfer matrices used in this work. The columns labeled $(0,0)$ and "Thermal" correspond to the expressions (A2) with $q=0$ and $q=1$, respectively. For the other columns, similar expressions may be worked out along the lines of Ref. [17].

Finally, let us remark that the computations for the generalized eight-vertex model introduced in Sec. VI B are produced from the same reference states, but slightly generalizing the transfer matrix to accommodate the contact-type vertices shown on Fig. 9.

[1] P.-G. de Gennes, *Scaling Concepts in Polymer Physics* (Cornell University Press, Ithaca, NY, 1979).
[2] B. Nienhuis, Phys. Rev. Lett. **49**, 1062 (1982).
[3] B. Maier and J. O. Rädler, Phys. Rev. Lett. **82**, 1911 (1999).
[4] H. W. J. Blöte and B. Nienhuis, J. Phys. A **22**, 1415 (1989).
[5] M. T. Batchelor, B. Nienhuis, and S. O. Warnaar, Phys. Rev. Lett. **62**, 2425 (1989).
[6] K. A. Dill *et al.*, Protein Sci. **4**, 561 (1995).
[7] P. J. Flory, Proc. R. Soc. London, Ser. A **234**, 60 (1956).
[8] G. I. Menon and R. Pandit, Phys. Rev. E **59**, 787 (1999).
[9] J. F. Nagle, Proc. R. Soc. London, Ser. A **337**, 569 (1974).
[10] R. J. Baxter, *Exactly Solved Models in Statistical Mechanics* (Academic Press, New York, 1982).
[11] P. D. Gujrati and M. N. Goldstein, J. Chem. Phys. **74**, 2596 (1981).
[12] A. Baumgartner and D. Yoon, J. Chem. Phys. **79**, 521 (1983).
[13] H. Saleur, J. Phys. A **19**, 2409 (1986).
[14] J. Bascle, T. Garel, and H. Orland, J. Phys. A **25**, L1323 (1992).
[15] M. L. Mansfield, Macromolecules **27**, 4699 (1994).
[16] We shall usually consider n_b and n_g real and non-negative, though we believe the model to have interesting properties for negative, or even complex, fugacities.
[17] J. L. Jacobsen and J. Kondev, Nucl. Phys. B **532**, 635 (1998).
[18] J. Kondev and C. L. Henley, Phys. Rev. B **52**, 6628 (1995).
[19] The vertex weights of the six-vertex model are conventionally called a, b, and c. We shall henceforth trade the variable c for w_X to avoid confusion with the central charge, which will play a major role in what follows.
[20] H. Orland, C. Itzykson, and C. de Dominicis, J. Phys. (France) Lett. **46**, 353 (1985).
[21] S. Higuchi, Nucl. Phys. B **540**, 731 (1999).
[22] J. Kondev, Phys. Rev. Lett. **78**, 4320 (1997).
[23] Vl. S. Dotsenko and V. A. Fateev, Nucl. Phys. B **240**, 312 (1984); **251**, 691 (1985).
[24] Note in particular that the field theory construction only applies to geometries that are isomorphic to the sphere with a point at infinity under a conformal transformation. Generalizations to higher genera have so far only been treated in mean-field theory [20,21].
[25] J. Cardy, *Scaling and Renormalization in Statistical Physics* (Cambridge University Press, Cambridge, 1996).
[26] B. Nienhuis, in *Phase Transitions and Critical Phenomena*, edited by C. Domb and J. L. Lebowitz (Academic, London, 1987), Vol. 11.
[27] H. W. J. Blöte, J. L. Cardy, and M. P. Nightingale, Phys. Rev. Lett. **56**, 742 (1986); I. Affleck, *ibid.* **56**, 746 (1986).
[28] J. L. Cardy, J. Phys. A **16**, L355 (1983).

[29] D. Kim and P. A. Pearce, J. Phys. A **20**, L451 (1987).
[30] J. L. Jacobsen and J. Kondev, J. Stat. Phys. **96**, 21 (1999).
[31] B. Duplantier and H. Saleur, Nucl. Phys. B **290**, 291 (1987).
[32] H. Saleur, J. Phys. A **19**, L807 (1986).
[33] S. Lise, A. Maritan, and A. Pelizzola, e-print cond-mat/9809210.
[34] B. Duplantier and H. Saleur, Phys. Rev. Lett. **59**, 539 (1987).
[35] R. Sedgewick, *Algorithms in C* (Addison-Wesley, Reading, MA, 1990).